How to Cite: Gulomjonov, Kh.A., Ashurov, N.Sh., Atakhanov, A.A., & Berdiyorov, G.R. (2026). Effect of HF Concentration on the Structural, Morphological, and Electrical Properties of $Ti_3C_2T_x$ MXene Prepared by Microwave-Assisted Etching. *Eurasian Journal of Chemistry, 31, 2(122), 77–90*. https://doi.org/10.31489/2959-0663/2-26-9

INORGANIC CHEMISTRY

Article

Received: 4 March 2026 | Revised: 18 May 2026 |
Accepted: 1 June 2026 | Published online: 2 June 2026

UDC 620.3:544.23

https://doi.org/10.31489/2959-0663/2-26-9

Khumoyunmirzo A. Gulomjonov[1*], Nurbek Sh. Ashurov[1], Abdumutolib A. Atakhanov[1], Golibjon R. Berdiyorov[2]

[1]*Institute of Polymer Chemistry and Physics, Tashkent, Uzbekistan;*
[2]*Hamad Bin Khalifa University, Doha, Qatar*
*(*Corresponding author's e-mail: khumoyungulomjonov@gmail.com)*

Effect of HF Concentration on the Structural, Morphological, and Electrical Properties of $Ti_3C_2T_x$ MXene Prepared by Microwave-Assisted Etching

Two-dimensional MXenes have emerged as a versatile class of materials for energy storage, electronics, and catalysis owing to their high electrical conductivity, tunable surface chemistry, and layered structure; however, the controlled synthesis of $Ti_3C_2T_x$ MXene with well-defined morphology and stable surface chemistry remains a major challenge, as etching conditions strongly influence structural integrity, degree of exfoliation, and functional performance. In this study, the morphological, structural, and functional evolution of $Ti_3C_2T_x$ MXene materials was systematically investigated by applying hydrofluoric acid (HF) etching at varying concentrations (6 %, 12 %, 24 %, 36 %, and 48 %) using microwave-assisted method. The impact of etching intensity on Al removal, layer delamination, and surface functionalization was examined through a multitechnique characterization approach including scanning electron microscopy (SEM), X-ray diffraction (XRD), Fourier transform infrared spectroscopy (FTIR), and energy-dispersive X-ray spectroscopy (EDS). The results reveal that an HF concentration of 24 % achieves efficient Al extraction while preserving the Ti–C framework, yielding well-exfoliated and structurally stable MXene sheets. Lower HF concentrations (6 % and 12 %) lead to incomplete etching and limited exfoliation, whereas higher concentrations (36 % and 48 %) cause over-etching and pronounced structural degradation. These findings underscore the critical role of etching conditions in tuning MXene morphology and functional properties. The ability to balance surface termination control and structural integrity via gradient etching is particularly relevant for the use of $Ti_3C_2T_x$ MXenes as conductive electrodes and interfacial layers in photovoltaic and other energy-conversion devices.

Keywords: $Ti_3C_2T_x$ MXene, MAX phase, gradient HF etching, etching concentration, surface terminations, exfoliation, morphology, structural integrity

Introduction

Two-dimensional (2D) transition metal carbides and nitrides, collectively known as MXenes, have rapidly emerged as an exciting class of nanomaterials due to their unique combination of metallic conductivity, hydrophilic surfaces, mechanical robustness, and versatile surface chemistries [1–3]. Since their discovery in 2011 via selective etching of the "A" layer from MAX phases ($M_{n+1}AX_n$), MXenes such as $Ti_3C_2T_x$ have attracted extensive research interest for applications including energy storage, catalysis, electromagnetic interference (EMI) shielding, sensing, and environmental remediation [4–6].

The conventional synthesis of MXenes involves chemical etching of the parent MAX phase using hydrofluoric acid (HF) or in situ generated HF from fluoride salts [7–10]. This process removes the "A" element (typically Aluminum), resulting in multilayered $Ti_3C_2T_x$ with surface terminations like –F, –OH, and –O, collectively denoted as T_x groups. These terminal groups strongly influence MXene's electrochemical, optical, and interfacial properties [11–14].

Theoretical and experimental studies have demonstrated that different surface terminations lead to distinct electronic, ionic, and optical behaviors in $Ti_3C_2T_x$ [15–21], significantly impacting their potential for energy storage, water purification, and membrane design. For instance, $Ti_3C_2T_x$ membranes with optimized surface terminations exhibit excellent ion-sieving and antibacterial capabilities, highlighting the key role of surface chemistry in functional performance [22–27].

The concentration of HF used during etching is a crucial parameter affecting MXene quality. Low HF concentrations often result in incomplete etching and poor delamination, whereas high HF concentrations promote over-etching, structural defects, and excessive fluorination, which degrade conductivity and mechanical integrity [28–30]. Excessive fluorination adversely affects selective ion intercalation and electrochemical behaviour, while oxygen terminations improve ion mobility and device performance [31–33].

To overcome the limitations of HF-based synthesis, alternative strategies such as in situ HF generation (e.g., LiF+HCl), molten salt etching, and electrochemical methods have been developed, allowing better control over surface terminations and morphology [34–36]. Moreover, hybrid structures combining MXenes with graphene or silver nanoparticles have been proposed to enhance membrane stability and electronic conductivity [37], demonstrating that post-synthesis modifications can synergistically improve properties when etching is well controlled. Furthermore, environmentally friendly approaches to MXene synthesis, particularly those based on microwave irradiation, are currently being actively developed [38, 39]. Microwave-assisted synthesis is reported to enhance reaction kinetics through rapid and uniform heating, thereby reducing processing time and improving etching efficiency compared to conventional methods [38–41]. These characteristics make microwave irradiation particularly suitable for controlled MXene synthesis. This technology offers several advantages, including cost-effectiveness, operational simplicity, rapid and uniform heating, high reaction rates, and improved control over morphology [40, 41]. In addition, microwave irradiation can promote selective and localized heating at the solid–liquid interface, which facilitates more effective disruption of Al layers and accelerates their removal from the Ti_3AlC_2 structure, contributing to improved etching uniformity and structural evolution of $Ti_3C_2T_x$ [42].

Recent advances in the MXene field have increasingly focused on engineering both the atomic surface terminations and multiscale architectures of $Ti_3C_2T_x$ and related systems to enhance their functional performance. In energy-storage applications, post-treatments such as atomic surface reduction have been shown to greatly improve capacitance and rate capability by optimizing termination chemistry and defect density [43, 44]. At the same time, the design of hierarchical MXene macrostructures including porous films, foams, and composite frameworks has enabled outstanding (EMI) shielding performance with high conductivity and mechanical robustness [45, 46]. Water-treatment and membrane technologies have also progressed rapidly, with MXene laminates and MXene–polymer hybrids demonstrating high desalination flux, ion-sieving selectivity, and antibacterial activity due to controlled interlayer spacing and surface surface terminations [47]. In the sensing field, $Ti_3C_2T_x$ based gas sensors have achieved high room-temperature sensitivity and selectivity by tuning defects, terminations, and hybridization with oxides or other 2D materials [48]. These developments are driven by rational synthesis control etching pathway, termination tuning, and structural design positioning MXenes as a versatile platform for next-generation supercapacitors, batteries, nanofluidic devices, sensors, and environmental remediation systems [49, 50].

Latest studies underscore that even after extensive exploration of MXenes, surface functionalization remains a pivotal lever for unlocking new application spaces and improving performance. By introducing tailored functional groups, ligands or dopants on the MXene surface, researchers have been able to modulate electronic work-function, wettability, interlayer spacing and defect states thereby improving properties for catalysis, sensing, biomedicine and energy storage [51–53]. For example, controlled termination engineering on $Ti_3C_2T_x$ enables precise tuning of the work function and charge-transfer kinetics, opening pathways to high-efficiency sensors and heterostructure devices [54]. In biomedicine and wearable electronics, surface-functionalized MXene platforms promise enhanced biocompatibility, selective binding and long-term stability in complex physiological environments something unmodified MXene surfaces alone struggle to deliver [55]. In electro-catalysis, the introduction of specific functional moieties on the MXene basal plane or edges improves active-site exposure and stabilises the material under harsh conditions, thus expanding MXene utility beyond its initial energy-storage niche [56]. Collectively, these advances reveal that surface functionalization isn't just a fine-tuning step, but a core strategy for diversifying MXene applications and achieving next-generation performance across domains.

The aim of this work was to systematically investigate the effect of hydrofluoric acid (HF) concentration on the morphological, structural, and functional evolution of $Ti_3C_2T_x$ MXene using a microwave-

assisted gradient etching approach. Unlike traditional HF etching, which relies solely on thermal conditions, this strategy accelerates reaction kinetics and allows for more precise control over the selective removal of aluminum from Ti_3AlC_2. The novelty of this work lies in the systematic investigation of HF concentration under microwave-assisted conditions, enabling the identification of a processing window where efficient Al removal, structural integrity, and controlled surface functionalization are simultaneously achieved. This study demonstrates that microwave irradiation facilitates the development of the characteristic accordion-like MXene morphology at 24 % HF, which suggests that microwave-assisted etching may enable efficient morphology formation at comparatively moderate HF concentrations. It establishes a quantitative structure–property correlation, linking shifts in the (002) reflection and increases in the c lattice parameter and interlayer spacing to the reaction yield and electrical conductivity of MXene and it identifies a practical processing window where efficient aluminum removal occurs while maintaining the integrity of the Ti–C framework, as higher HF concentrations lead to over-etching and structural degradation. These findings provide a rational basis for tailoring the morphology and functional properties of $Ti_3C_2T_x$ MXenes through controlled etching conditions. In the present work, a direct experimental comparison with conventional non-microwave HF etching was not performed; however, the role of microwave irradiation is discussed based on literature reports and the observed formation of accordion-like $Ti_3C_2T_x$ morphology at 24 % HF.

Experimental

Chemicals and Materials

MAX phase (Ti_3AlC_2, powder, 98 wt%) was purchased from Shandong Fan Tai Fine Chemical Biotechnology Co., Ltd., China. Hydrofluoric acid (HF, 48 wt %) was purchased from Sigma-Aldrich Chemical Co. Ltd. (Tianjin, China). Filtration and delamination processes employed cellulose acetate membranes with a pore size of 0.22 μm (GVS). All reagents were of analytical grade and used without further purification. Deionized water was employed throughout all experiments unless otherwise stated.

Synthesis of $Ti_3C_2T_x$ (MXene)

$Ti_3C_2T_x$ was synthesized by selective chemical etching of the Al layer from the Ti_3AlC_2 using a published method with a slight modification [57]. Briefly, 1 g of Ti_3AlC_2 powder was added to 10 mL of hydrofluoric acid solutions of varying concentrations (6 %, 12 %, 24 %, 36 %, and 48 %). The mixtures were placed into a Microwave Digester (BMD-12H, China) and treatment with microwave radiation at 2450 MHz for 30 minutes. Following the microwave treatment, the suspensions were centrifuged at 3500 rpm for 10 minutes, and the black powder was separated. The sediments were washed repeatedly with deionized (until pH ≈ 6-7) to remove residual HF. To obtain delaminated MXene powders, the washed sediments were mildly sonicated for 30 minutes. The final $Ti_3C_2T_x$ powders were collected by vacuum drying at 60 °C for 12 hours. MXene samples synthesized using 6 %, 12 %, 24 %, 36 %, and 48 % HF solution were labeled as MX-6, MX-12, MX-24, MX-36 and MX-48, respectively.

Although it is not possible to calculate an accurate reaction yield because it isn't possible to define an exact stoichiometry for the samples obtained, a yield was calculated by the following formula, that usually is used in literature for these materials [58]:

$$\text{Yield}(\%)=\left(\frac{\text{MXene mass}}{\text{MAX phase mass}}\right)\times 100.$$

Characterization Methods

FTIR

The FTIR spectrometer "Inventio-S" (Bruker) was used and FTIR spectra were recorded in 400–4000 cm^{-1} wavenumber range with a resolution of 2 cm^{-1} and 32 scans at a temperature of 25 °C. All samples were finely ground, dried at 60 °C for 12 h, and pressed into KBr pellets (1 wt%) before analysis. Software of OPUS was applied to determine the peaks at specific points.

Wide-Angle X-Ray Diffraction

XRD studies were carried out using XRD Miniflex 600 (Rigaku, Japan) with monochromatic CuKα radiation isolated by a nickel filter with a wavelength of 1.5418 Å at 40 kV and the current strength of 15 mA. The spectrum was recorded in the interval $2\theta = 5°–40°$. The air-dried MXene powders were gently ground, mounted on zero-background glass slides, and analyzed under identical sample thickness and humidity conditions. The data processing of experimental diffraction patterns, peak deconvolution, describing the peaks

used by Miller indices, peak shape, and the basis for the amorphous contribution were conducted using the software "SmartLab Studio II" and data base PDF-2 (2020 Powder diffraction file, ICDD).

Scanning Electron Microscopy (SEM)

Scanning electron microscopy studies were performed using SEM equipment Jeol-210 (Japan). Magnification of the device ×10–300000, voltage 200–300 V, maximum scanning area ($x \div y \div z$) is 120÷120÷65 μm. SEM images were obtained at an accelerating voltage of 10 kV and a working distance of 10.6 mm.

Conductivity

The electrical conductivity of MXene and MAX phases samples was evaluated from measured sheet resistance using the Ossila four-point probe system (Osilla, UK), combined with thickness measurements to calculate conductivity. Four-point probe measurements were performed following the procedures described in [59].

Statistical Analysis

All experimental data were collected in triplicates and data expressed as average ± standard deviation. Data were compared using a one-way ANOVA with post-Bonferroni test using GraphPad Prism 5.04 (GraphPad Software Inc.)

Results and Discussion

$Ti_3C_2T_x$ MXene was synthesized through selective chemical etching of the aluminum layers in the parent MAX phase Ti_3AlC_2 using hydrofluoric acid (HF) at various concentrations. This etching process occurs due to the preferential reactivity of aluminum with HF, resulting in the formation of soluble AlF_3 species and the release of hydrogen gas (H_2), while the titanium-carbon framework remains largely intact. Consequently, the layered structure of Ti_3C_2 is preserved, and surface terminations such as –F, –OH, and –O are introduced, resulting in $Ti_3C_2T_x$ (Fig. 1).

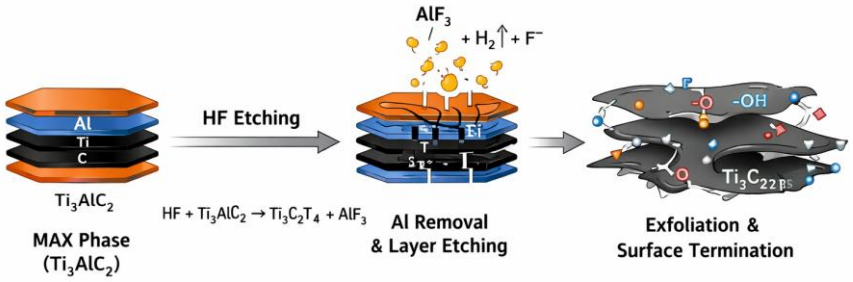

Figure 1. Schematic representation of MXene preparation via selective chemical etching process

In the FTIR spectrum of pristine, non-etched Ti_3AlC_2 (Fig. 2, curve 1), the weak absorption bands are observed, indicating the absence of significant surface functionalization. A broad, low-intensity band in the 3443–3439 cm^{-1} region corresponds to O–H stretching vibrations. The bands at 2854 and 2925 cm^{-1} arise from C–H stretching vibrations, likely associated with trace organic residues remaining from the synthesis process, while the weak band near 1640 cm^{-1} is assigned to the bending vibration of adsorbed water molecules, attributed to their hydrophilic nature [60]. In the low wavenumber region (500–800 cm^{-1}), characteristic vibrations of Ti–C and Ti–Al bonds dominate, which are typical of Ti-based MAX phases and confirm that the layered Ti_3AlC_2 structure is preserved with negligible surface terminations.

For the sample MX-6 (Fig. 2, curve 2), a noticeable broadening and increase in intensity of the O–H stretching band at ~3440 cm^{-1} is observed, indicating the initial formation of hydroxyl groups on the MXene surface. At the same time, weak new features appearing in the 550–650 cm^{-1} region indicate the onset of Ti–O bond formation. When the HF concentration is increased to 12 % and 24 %, the intensity of the O–H stretching band increases significantly, reflecting a higher density of hydroxyl terminations. In addition, absorption bands in the 1200–1400 cm^{-1} region, assigned to C–F stretching vibrations, indicate the progressive incorporation of fluorine terminations. Notably, for the sample MX-24 (Fig. 2, curve 4), a balanced intensity of O–H and C–F groups is observed, together with clear Ti–O/Ti–F vibrations in the low-wavenumber region [61]. This behaviour indicates that the Al layers were effectively removed while the Ti–C backbone of the structure remained intact. With further increase of the HF concentration to 36 % and 48 %, an intense O–H stretching band is also observed; however, the comparison of absolute intensities between different KBr

tablets is semi-quantitative due to different water sorption. The enhanced intensity of the band near 1640 cm^{-1} is attributed to a higher degree of water molecule intercalation between the MXene layers. However, the appearance of distinct Ti–F vibrations in the 550–650 cm^{-1} region for these samples indicates excessive fluorine coverage of the surface. This observation is consistent with the structural degradation and over-etching effects revealed by SEM and XRD analyses.

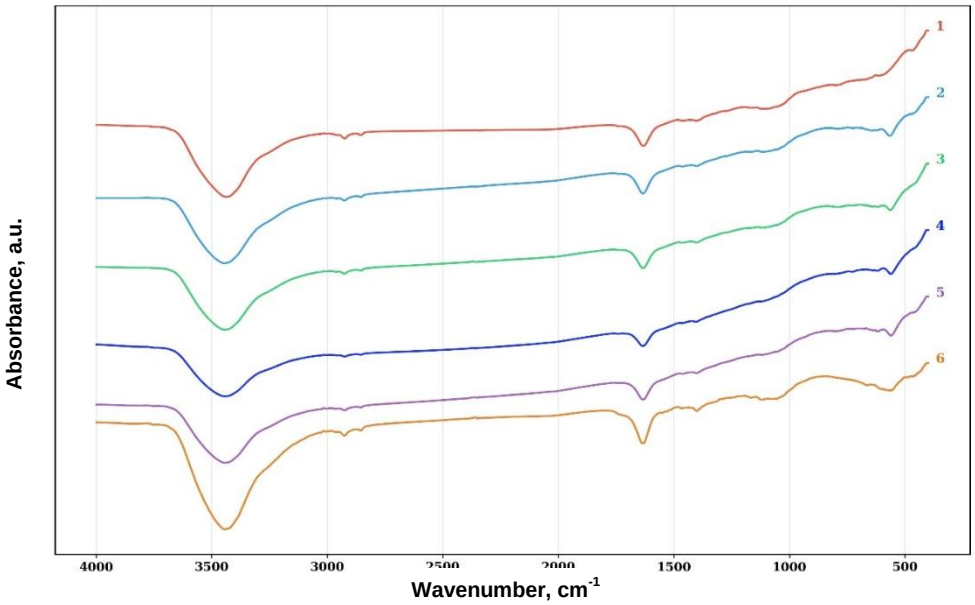

Figure 2. FTIR spectra of MAX phase (*1*) and MXene samples:
MX-6 (*2*), MX-12 (*3*), MX-24 (*4*), MX-36 (*5*), MX-48 (*6*)

Overall, the FTIR analysis indicates that HF concentration influences the evolution of surface-related functional groups on $Ti_3C_2T_x$ MXene. Since FTIR provides qualitative information on vibrational features, the observed band intensities are discussed as relative trends rather than precise quantitative measurements. While incomplete functionalization is observed at low concentrations, an optimal ratio of –OH, –F, and =O groups is achieved at an intermediate concentration (24 %). Higher HF concentrations, however, lead to excessive fluorination, which may compromise the structural stability of the material.

The structural changes occurring during HF etching of Ti_3AlC_2 and the subsequent formation of $Ti_3C_2T_x$ MXene were investigated using XRD (Fig. 3*a*). The neat Ti_3AlC_2 sample exhibits sharp and intense diffraction peaks characteristic of the MAX phase, confirming its high crystallinity and well-ordered layered structure. The (002) peak observed at a low angle (~9.49°) corresponds to the regular stacking of Ti–C layers separated by Al atomic layers, including characteristic peaks around 2θ = 19.2° (004), 29.5° (103/006), 36.4° (104), 39.2° (105), and 42.3° (106) [62].

After HF etching, significant changes are observed in the diffraction patterns of all $Ti_3C_2T_x$ samples. For the sample MX-6, the (002) peak shifts to a lower 2θ value, indicating an increase in interlayer spacing, which is commonly attributed to partial Al removal and is often accompanied by the formation of surface functional groups. The persistence of a few residual MAX-phase peaks, such as the (104) reflection at ~39°, indicates that etching was not fully complete and exfoliation of the MAX phase is limited. When the HF concentration is increased to 12 %, Al-related peaks further weaken and the (002) peak becomes more pronounced at ~9.26°. This indicates more effective Al removal and partial opening of the layered structure; however, traces of the MAX phase are still present, confirming that the etching process is not yet complete. At low HF concentrations (6 % and 12 %), the etching reaction proceeds slowly and incompletely. SEM and XRD results indicate that a significant fraction of the Al layers remains within the structure, which limits interlayer expansion and suppresses effective layer separation. The persistence of MAX-phase reflections in XRD patterns and the relatively compact layered morphology observed by SEM confirm that insufficient etching hinders the formation of well-separated MXene sheets (Fig. 4*b*, *c*). In this regime, the Ti_3AlC_2 structure is only partially transformed, resulting in limited layer separation and structurally heterogeneous products.

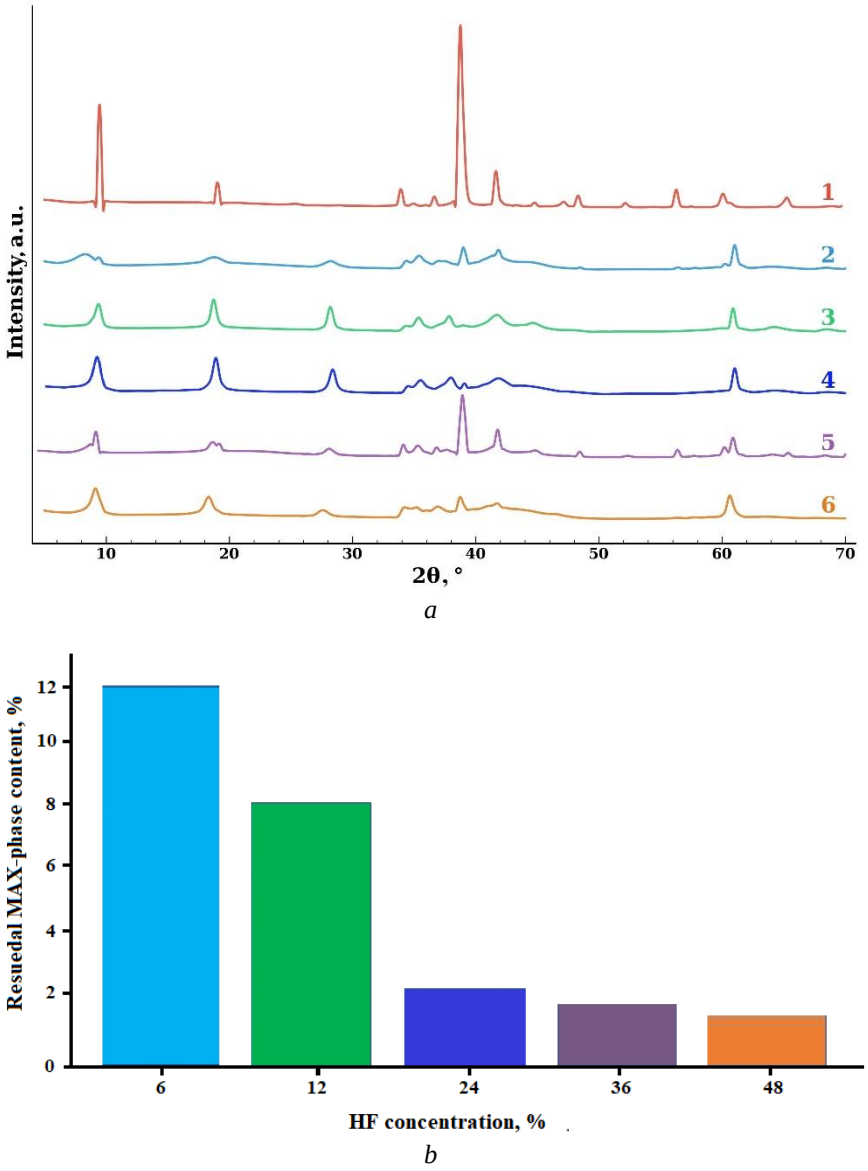

Figure 3. XRD patterns (*a*) of MAX-phase (*1*) and MXene samples: MX-6 (*2*), MX-12 (*3*), MX-24 (*4*), MX-36 (*5*), MX-48 (*6*); Residual MAX-phase content of etched samples at different HF concentration, determined from XRD analysis (*b*)

The most obvious structural transformation is observed in the sample MX-24. The XRD pattern shows a strong and well-defined (002) MXene peak at ~9.21°, indicating successful conversion from Ti_3AlC_2 MAX phase, while the characteristic MAX-phase reflections, such as (104) at ~39° and (105) at ~41°, have nearly vanished. The observed shift of the (002) peak, which is often the result of delamination or intercalation, may also be related to the etching process. It is possible that functional groups such as –F, –OH, and =O formed during etching can increase the interlayer spacing [63]. Increasing the HF concentration to an intermediate level (24 %) results in efficient and selective Al removal. The disappearance (or significant weakening) of the (104) peak of the MAX phase and a pronounced shift of the (002) reflection to smaller angles confirm successful etching and expansion of the interlayer space. The disappearance (or strong attenuation) of the MAX-phase (104) peak and the pronounced shift of the (002) reflection to lower angles in XRD patterns indicate successful etching and interlayer expansion. SEM observations reveal a typical accordion-like multilayer morphology, characteristic of well-formed MXene (Fig. 4*d*). At this concentration, the Ti–C framework remains structurally stable, while the surface becomes functionalized by –F, –OH, and –O groups originating from the etching medium and subsequent washing steps. This balance between Al removal and framework preservation results in structurally intact, multilayer $Ti_3C_2T_x$ with expanded interlayer spacing.

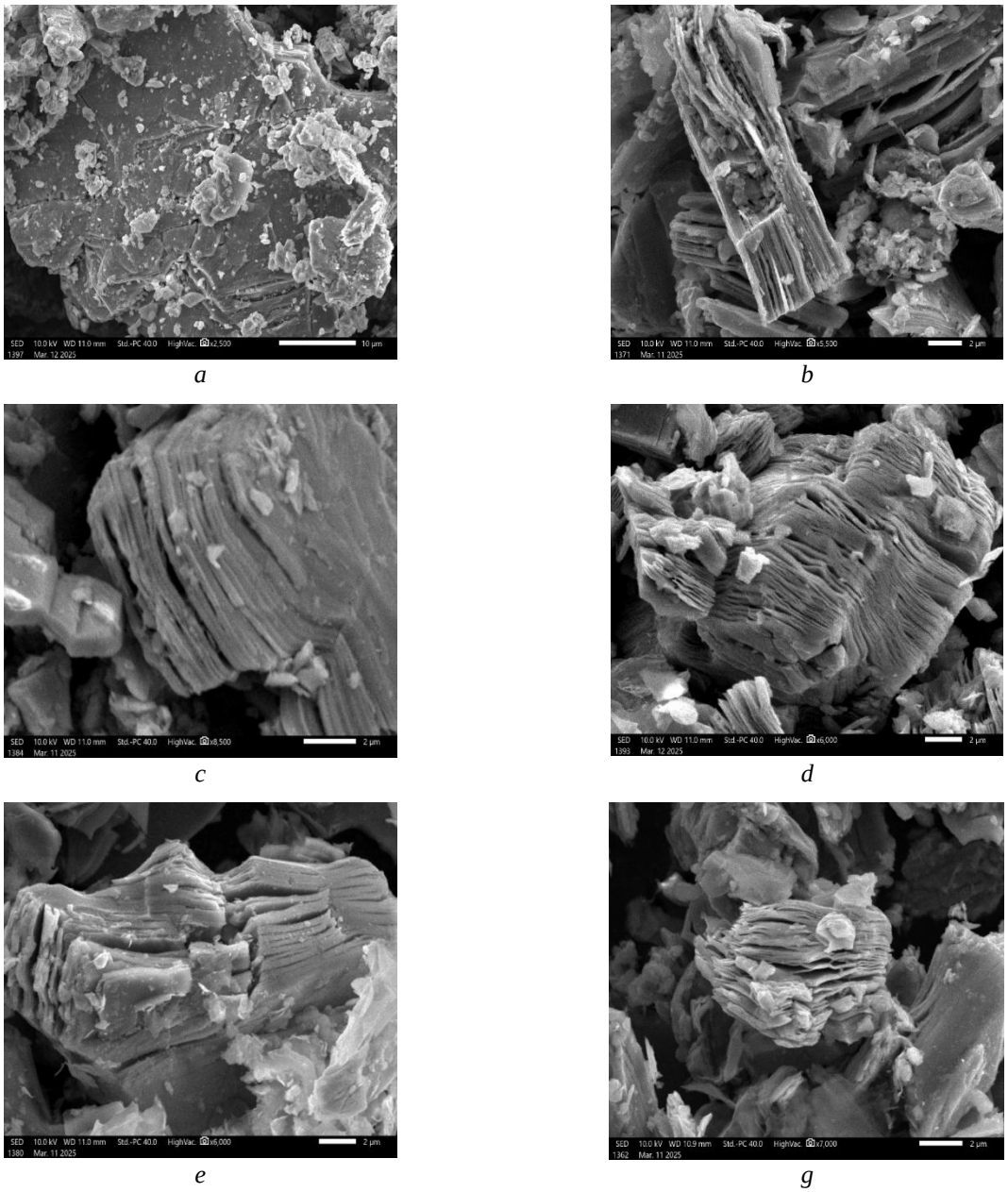

Figure 4. SEM images of MAX (*a*) and MXene samples: *b*) MX-6; *c*) MX-12; *d*) MX-24; *e*) MX-36; *g*) MX-48

XRD patterns of MX-36 and MX-48 show peak broadening and a decrease in intensity. These features indicate structural disorder, defect formation, and partial degradation of the Ti–C framework. Although weaker MXene peaks, such as (004) and (006), remain detectable, the intensity reduction indicates a significant loss of long-range structural order. At higher HF concentrations (36 % and 48 %), the etching becomes overly aggressive. Although Al is completely removed, excessive chemical attack leads to partial degradation of the Ti_3C_2 layers, generation of structural defects, and possible thinning or fragmentation of the sheets. This over-etching is reflected in the deterioration of the layered morphology in SEM images (Fig. 4*e*, *f*) and the broadening or weakening of characteristic MXene diffraction peaks in XRD patterns. In addition, stronger fluorination at high HF concentrations increases the density of –F terminations, which may adversely affect electrical conductivity and mechanical integrity [64].

As the HF concentration increased from 6 to 48 %, the (002) reflection gradually shifted to lower angles (from 9.30° to 9.07°), indicating an increase in the c lattice parameter from 18.85 to 21.08 Å and an expansion of the interlayer spacing from 9.7 to 13.0 Å (Tab. 1).

Table 1

Structural parameters, yield and conductivity of samples

Sample	*a*, Å	*c*, Å	2θ, °	Interlayer spacing, Å	Yield, %	Conductivity, S m^{-1}
MX-6	3.08	18.85	9.30	9.7	65	14400
MX-12	3.08	19.55	9.26	10.2	68	16500
MX-24	3.07	20.51	9.21	12.2	72	19200
MX-36	3.06	21.02	9.17	12.6	70	22300
MX-48	3.08	21.08	9.07	13.0	67	23800

The evolution of the low-angle (002) reflection can be interpreted in three complementary aspects. First, the progressive attenuation/disappearance of characteristic MAX reflections (e.g., around ~39–41°) evidences the gradual conversion of Ti_3AlC_2 to $Ti_3C_2T_x$ as the HF concentration increases. Second, the shift of the (002) reflection towards lower 2θ values together with the increase of the c lattice parameter (Tab. 1) indicates interlayer expansion, which can arise from Al removal and the introduction of surface species and interlayer water during washing. Third, at high HF concentrations (36–48 %), the pronounced broadening and intensity loss of the (002) and higher-order peaks suggest increased structural disorder and defect generation, consistent with over-etching effects observed by SEM. Importantly, in this work no dedicated intercalation chemistry (e.g., Li^+-intercalation [65]) was applied; therefore, the observed basal-spacing changes associated with interlayer expansion are attributed primarily to etching-induced structural evolution and surface functionalization rather than deliberate intercalation-driven delamination.

This structural evolution was accompanied by a steady increase in MXene yield (from 65 % to 72 %) and electrical conductivity of the corresponding films from 1.44×10^4 to 2.38×10^4 S m^{-1} with increasing HF concentration (Tab. 1), which corresponds to 144–238 S cm^{-1}. It should be noted that the conductivity of $Ti_3C_2T_x$ films reported in the literature [34, 66] spans a broad range depending on the etching route, oxidation state, flake size distribution, film density, and post-treatments (e.g., pressing, annealing, surface reduction). In this work, the films were prepared without additional densification, high-temperature annealing, or chemical reduction, therefore the obtained values are expected to fall into a moderate conductivity regime. Importantly, the consistent increase in conductivity correlates with the structural evolution revealed by XRD (increasing c parameter and interlayer spacing), indicating that more efficient Al removal and improved delamination reduce the interflake contact resistance and promote better stacking/alignment of conductive flakes in the film. At the highest HF concentrations (36–48 %), the conductivity continues to increase; however, SEM and XRD indicate the onset of structural degradation/over-etching, which suggests that further optimization should balance conductivity gains against the preservation of sheet integrity.

Figure 3*b* illustrate the effect of HF concentration on the phase purity; increasing the HF concentration leads to a significant decrease in the residual Ti_3AlC_2 content: approximately 12 % at MX-6, 8 % at MX-12, 2 % at MX-24, 1.5 % at MX-36 and a minimum of 1 % at MX-48.

Overall, the XRD results demonstrate that HF concentration plays a critical role in controlling the etching efficiency and structural integrity of MXene. Low HF concentrations lead to incomplete Al removal, whereas excessive HF results in structural degradation. Among the investigated conditions, HF concentrations in the range of 24 % are considered optimal for producing well-exfoliated and structurally stable MXene. These findings are in good agreement with the SEM, FTIR, and EDS analyses.

The smooth and dense surface, along with the absence of layer separation or significant structural defects, can be attributed to the strong interlayer bonding characteristic of the MAX phase (Fig. 4*a*). EDS results provided a semi-quantitative estimation of the elemental composition, showing Ti, Al, and C as the dominant elements with approximate values of 73.75 wt%, 18.20 wt%, and 8.04 wt%, respectively (Figure 5*a*), which are in reasonable agreement with the expected composition of the Ti_3AlC_2 MAX phase [67]. Importantly, fluorine (F) and oxygen (O) were not detected in this sample, indicating the absence of surface terminationsprior to etching. This confirms that the Ti_3AlC_2 phase has a chemically inert and stable surface.

After etching the MAX phase with 6 % HF, initial changes on the material surface were observed (Fig. 4*b*). SEM images revealed shallow pits and small voids, indicating the onset of the etching process. Interlayer expansion was still very limited, and the overall structural integrity remained largely intact. EDS analysis suggests an apparent decrease in the Ti signal to approximately 68.70 wt%, along with a marked decrease in the Al signal. (Fig. 5) The apparent increase in the carbon signal to approximately 13.96 wt% may be related to the relative enrichment of the Ti–C framework following Al removal. Additionally, the

detected fluorine (~11.31 wt%) and oxygen (~6.03 wt%) signals in the EDS spectrum suggest the formation of fluorine- and oxygen-containing surface species through interaction with HF. These groups likely play an important role in enhancing the hydrophilicity and chemical reactivity of the MXene surface [68]. Minor Ti loss and partial exfoliation were not clearly visible in the SEM images, and these phenomena were primarily confirmed through elemental analysis.

At 12 % HF, the etching process became more pronounced. It was observed the partial separation of layers and loosely packed lamellar structures, suggesting further Al removal and partial formation of MXene (Fig.4*c*). Full delamination had not yet occurred, as the layers remained partially aggregated. EDS analysis suggests an apparent increase in the Ti signal to approximately 73.65 wt%, which may reflect the exposure of additional Ti_3C_2 layers after Al removal. Meanwhile, the C content slightly decreased to 11.14 wt%, possibly due to partial surface restructuring or degradation. The detected F (~10.15 wt%) and O (~4.76 wt%) signals remained noticeable, suggesting continued surface functionalization. This sample represents a transitional stage between partial etching and optimal exfoliation.

The sample M-24 exhibited the most favourable structural and chemical characteristics. SEM images revealed the characteristic "accordion-like" morphology of MXenes, with significantly expanded interlayer spacing. A similar "accordion-like" morphology of MXenes was also observed in Ref. [69] when the MAX phase was etched using a 30 % HF solution. In our case, the development of this morphology at an HF concentration of 24 % can be attributed to the use of microwave irradiation, which enhances the reaction kinetics and allows efficient etching at a comparatively lower etchant concentration [41].

This morphology is particularly beneficial for applications requiring a high surface area, such as energy storage or catalysis. Although some regions still showed partial interlayer cohesion, the overall structure was well exfoliated. EDS analysis showed an apparent high Ti signal (~76.74 wt%) among the samples, supporting the preservation of the Ti–C framework (Fig. 5). The detected F (~8.55 wt%) and O (~4.47 wt%) signals suggest relatively balanced surface functionalization. This sample represents the optimal balance between effective Al removal, structural stability, and surface functionalization.

At 36 % HF concentration, significant changes in morphology and chemistry were observed. Partial collapse of lamellar structures, excessive widening of interlayer gaps, and local distortions were observed (Fig. 4*e*). Although expanded layers remained, mechanical integrity began to deteriorate. EDS analysis suggests that the Ti signal remained relatively high (~76.94 wt%), while the apparent C signal decreased to approximately 7.03 wt%, which may indicate partial degradation of the carbon framework. The F signal increased to approximately 9.61 wt%, while the O signal appeared very low (~0.03 wt%); however, these values should be interpreted with caution due to the limited accuracy of EDS for light elements.

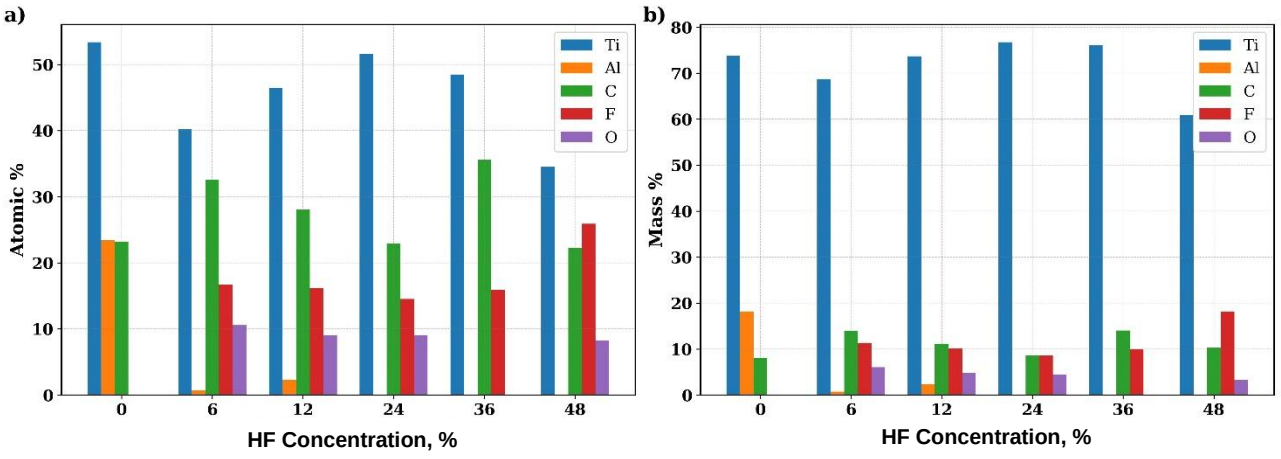

Figure 5. (*a*) Atomic percentage of Ti, Al, C, F and O in MAX phase Ti_3AlC_2 and $Ti_3C_2T_x$ samples etched at different HF concentrations obtained from EDS analysis; (*b*) Mass percentage of corresponding elements as a function of HF concentration

With 48 % HF, the sample showed severe alterations in both morphology, elemental composition and size. SEM images revealed well-separated, thin, and smooth lamellar sheets, indicating high exfoliation. EDS results suggest substantial compositional changes: the Ti signal decreased to approximately 60.93 wt%, while the F (~18.15 wt%) and O (~8.27 wt%) signals increased markedly, suggesting over-functionalization

(Fig. 5). Excessive etching led to surface passivation, which could significantly impair the electrochemical properties of the material.

The SEM observations are consistent with the XRD-derived structural evolution and the electrical conductivity trend. At low HF concentrations (6–12 %), the limited layer separation and the presence of residual MAX reflections indicate incomplete etching, which likely results in heterogeneous stacking and higher interflake contact resistance in films. At intermediate HF concentration (24 %), the formation of a well-developed accordion-like architecture indicates effective Al extraction and opening of interlayer galleries, while XRD still shows comparatively preserved structural order and EDS suggests relatively balanced F/O signals. This condition provides the best overall balance between phase conversion, structural integrity, and controlled surface functionalization, which is reflected in the highest yield (72 %) among the studied conditions and a notable conductivity increase relative to MX-6 and MX-12. In contrast, at higher HF concentrations (36–48 %), SEM and XRD evidence increasing disorder/fragmentation (peak broadening and morphology deterioration), suggesting over-etching that may compromise mechanical integrity despite higher conductivity. Therefore, MX-24 is identified as the most practical synthesis condition when both structural preservation and functional performance are considered. Although the highest electrical conductivity is observed for the 48 % HF sample, this condition is associated with increased structural disorder and over-etching effects. In contrast, the 24 % HF sample provides the best overall balance between structural integrity, controlled surface functionalization, morphology, yield, and electrical performance.

FTIR and EDS results indicate the formation of surface-containing species (e.g., oxygen- and fluorine-containing groups) after HF treatment; however, these methods do not provide a complete chemical-state assignment of the $Ti_3C_2T_x$ surface. FTIR reflects vibrational features that can overlap, and EDS is semi-quantitative and does not distinguish bonding configurations. The apparent discrepancy between EDS and FTIR results can be attributed to the limited sensitivity of EDS for detecting low concentrations of light elements and the fact that FTIR detects vibrational features of surface functional groups rather than bulk composition. Therefore, the discussion of –F/–OH/–O terminations in this work is presented as qualitative evidence of termination evolution with etching conditions, while more definitive chemical-state identification would require complementary XPS analysis.

In summary, SEM and EDS analyses demonstrate the critical effect of HF concentration on the morphological, yield and conductivity of $Ti_3C_2T_x$ MXene. 24 % HF provided the optimal balance, ensuring effective Al removal, controlled surface functionalization, and high structural integrity. Lower concentrations (6 % and 12 %) were insufficient for full exfoliation, while higher concentrations (36 % and 48 %) resulted in over-functionalization and structural degradation. These findings highlight the importance of carefully optimizing etching conditions for MXene applications in energy storage, catalysis, and sensing.

Conclusions

$Ti_3C_2T_x$ (MXene) was successfully synthesized from Ti_3AlC_2 (MAX phase) by selective etching in hydrofluoric acid (HF) solutions with different concentrations (6 %, 12 %, 24 %, 36 %, and 48 %) using a microwave-assisted approach. The obtained samples were comprehensively characterized by FTIR, XRD, SEM, and EDS techniques.

FTIR spectra indicated the presence of various surface-related species on the MXene layers. Samples etched at lower HF concentrations (6 % and 12 %) exhibited relatively more visible O–H vibrational features, whereas those treated at higher HF concentrations (36 % and 48 %) were dominated by bands associated with F- and O-containing groups, highlighting the strong influence of etching conditions on the surface chemistry of MXene. XRD analysis revealed a systematic shift and broadening of the characteristic (002) reflection near $2\theta \approx 9.5°$, indicating an increase in the interlayer spacing and partial structural disordering. This effect became more pronounced for the MX-24, MX-36, and MX-48 samples, confirming progressive etching and structural transformation of the MAX phase.

SEM observations showed that increasing HF concentration led to a more pronounced separation of the layered structure. At higher HF concentrations (36–48 %), stronger etching led to more pronounced interlayer opening; however, this was accompanied by peak broadening, structural disorder, and partial degradation of the Ti–C framework, indicating over-etching rather than improved structural quality. EDS analysis further demonstrated a significant decrease in aluminum content with increasing HF concentration, accompanied by an increase in fluorine and oxygen contents, which is consistent with progressive surface functionalization of $Ti_3C_2T_x$.

Overall, this work not only provides a systematic assessment of the effect of HF concentration on the formation of $Ti_3C_2T_x$ MXene, but also highlights the effectiveness of microwave-assisted etching in overcoming kinetic limitations of the selective etching process. The identified processing window and the established structure–property correlations offer practical guidelines for tailoring $Ti_3C_2T_x$ MXenes for conductive film and interfacial layer applications.

Funding

This research was supported by the Basic Fundamental Program of the Academy of Sciences of the Republic of Uzbekistan, and the Project "Biomass-based composite fibers for non-woven fabric with electromagnetic interference shielding" supported by the Korea International Cooperation Agency (KOICA).

*Author Information**

**The authors' names are presented in the following order: First Name, Middle Name and Last Name*

Khumoyunmirzo Adkhamjon o'gli Gulomjonov (*corresponding author*) — Junior Researcher, Institute of Polymer Chemistry and Physics, Abdulla Kadiri Street, 7-b, 100128, Tashkent, Uzbekistan; e-mail: khumoyungulomjonov@gmail.com; https://orcid.org/0009-0005-0330-0097

Nurbek Shodievich Ashurov — Candidate of Physical and Mathematical Sciences, Senior Researcher, Institute of Polymer Chemistry and Physics, Abdulla Kadiri street, 7-b, 100128, Tashkent, Uzbekistan; e-mail: ansss72@mail.ru; https://orcid.org/0000-0001-5246-434X

Abdumutolib Abdupatto o'g'li Atakhanov — Doctor of Technical Sciences, Professor, Director of Institute of Polymer Chemistry and Physics, Abdulla Kadiri Street, 7-b, 100128, Tashkent, Uzbekistan; e-mail: a-atakhanov@yandex.com; https://orcid.org/0000-0002-4975-3658

Golibjon Rakhmatullaevich Berdiyorov — Senior Scientist, Energy Center, Qatar Environment and Energy Research Institute, Hamad Bin Khalifa University, P.O Box 5825, Doha, Qatar; e-mail: gberdiyorov@hbku.edu.qa; https://orcid.org/0000-0003-4483-4800

Author Contributions

The manuscript was written through contributions of all authors. All authors have given approval to the final version of the manuscript. CRediT: **Khumoyunmirzo Adkhamjon o'gli Gulomjonov** writing — original draft; **Nurbek Shodievich Ashurov** writing — original draft, conceptualization; **Abdumutolib Abdupatto o'g'li Atakhanov** conceptualization, supervision; **Golibjon Rakhmatullaevich Berdiyorov** writing — original draft, formal analysis, investigation, methodology.

Conflicts of Interest

The authors declare no conflict of interest.

References

1 Naguib, M., Kurtoglu, M., Presser, V., Lu, J., Niu, J., Heon, M., Hultman, L., Gogotsi, Y., & Barsoum, M. (2011). Two-dimensional nanocrystals produced by exfoliation of $Ti_3C_2T_x$. *Advanced Materials,* 23, 4207. https://doi.org/10.1002/adma.201190147

2 Anasori, B., Lukatskaya, M.R., & Gogotsi, Y. (2017). 2D metal carbides and nitrides (MXenes) for energy storage. *Nature Reviews Materials,* 2, 16098. https://doi.org/10.1038/natrevmats.2016.98

3 Vahid Mohammadi, A., Rosen, J., & Gogotsi, Y. (2021). The world of two-dimensional carbides and nitrides (MXenes). *Science*, 372(6547). https://doi.org/10.1126/science.abf1581

4 Lei, J.C., Zhang, X., & Zhou, Z. (2015). Recent advances in MXene: preparation, properties, and applications. *Frontiers of Physics*, 10, 276–286. https://doi.org/10.1007/s11467-015-0493-x

5 Alhabeb, M., Maleski, K., Anasori, B., Lelyukh, P., Clark, L., Sin, S., & Gogotsi, Y. (2017). Guidelines for synthesis and processing of 2D titanium carbide ($Ti_3C_2T_x$) MXene. *Chemistry of Materials,* 29, 7633–7644. https://doi.org/10.1021/acs.chemmater.7b02847

6 Krishnaiah, P., Awan, H., Walvekar, R., & Manickam, S. (2022). MXene-based composites and their applications. In: MXene Materials. *Springer,* 4, 53–86. https://doi.org/10.1007/978-3-031-05006-0_4

7 Mashtalir, O., Naguib, M., Mochalin, V.N., Dall'Agnese, Y., Heon, M., Barsoum, M.W., & Gogotsi, Y. (2013). Intercalation and delamination of layered carbides and carbonitrides. *Nature Communications*, 4, 1716. https://doi.org/10.1038/ncomms2664

8 Nouseen, S., & Pumera, M. (2025). Electrochemical etching of MXenes: mechanism, challenges and future outlooks. *Journal of Materials Chemistry A*, 13, 34055–34084. https://doi.org/10.1039/D5TA04176G

9 Rahman, U.U., Humayun, M., Ghani, U., Usman, M., Ullah, H., Khan, A., El-Metwaly, N., & Khan, A. (2022). MXenes as emerging materials: synthesis, properties, and applications. *Molecules*, 27, 4909. https://doi.org/10.3390/molecules27154909

10 Peng, Y.Y., Akuzum, B., Kurra, N., Zhao, M., Alhabeb, M., Anasori, B., & Gogotsi, Y. (2016). All-MXene solid-state microsupercapacitors for on-chip energy storage. *Energy & Environmental Science*, 9, 2847–2854. https://doi.org/10.1039/C6EE01717G

11 Khazaei, M., Arai, M., Sasaki, T., Chung, C.Y., Estili, M., Sakka, Y., & Kawazoe, Y. (2013). Novel electronic and magnetic properties of two-dimensional transition metal carbides and nitrides. *Advanced Functional Materials*, 23, 2185–2192. https://doi.org/10.1002/adfm.201202502

12 Khanal, R., & Irle, S. (2023). Effect of surface functional groups on MXene conductivity. *Journal of Chemical Physics*, 158, 124703. https://doi.org/10.1063/5.0141589

13 Rafique, M., Tahir, M., & Anwar, S. (2024). MXenes for energy storage applications. In *MXene Materials*. CRC Press. https://doi.org/10.1201/9781003465768

14 Mozafari, M., & Soroush, M. (2021). Surface functionalization of MXenes. *Materials Advances*, 2, 7277–7291. https://doi.org/10.1039/D1MA00625H

15 Yang, G., Yao, X., Li, Y., Hu, Y., Chen, X., Li, J., Chen, J., & Jiang, J. (2023). $Ti_3C_2T_x$ MXene Nanosheet-Based Hybrid Films for Enhanced Wave Absorption-Dominated Electromagnetic Interference Shielding. *ACS Applied Nano Materials*, 6(20), 19378–19391. https://doi.org/10.1021/acsanm.3c03932

16 Berdiyorov, G. (2015). Effect of lithium and sodium ion adsorption on electronic transport properties of Ti_3C_2 MXene. *Applied Surface Science*, 359, 153–158. https://doi.org/10.1016/j.apsusc.2015.10.050

17 Berdiyorov, G., & Mahmoud, K. (2017). Effect of surface termination on ion intercalation selectivity of bilayer $Ti_3C_2T_x$ MXene. *Applied Surface Science*, 416, 980–986. https://doi.org/10.1016/j.apsusc.2017.04.195

18 Berdiyorov, G. R. (2016). Optical properties of functionalized $Ti_3C_2T_2$ (T = F, O, OH) MXene: First-principles calculations. *AIP Advances*, 6(5). https://doi.org/10.1063/1.4948799

19 Rasool, K., Pandey, R., Rasheed, P.A., Berdiyorov, G., & Mahmoud, K. (2019). MXenes for environmental and water treatment applications. In: *MXenes.* Springer. https://doi.org/10.1007/978-3-030-19026-2_22

20 Rasool, K., Mahmoud, K., Johnson, D.J., Helal, M.I., Berdiyorov, G., & Gogotsi, Y. (2017). Efficient antibacterial membrane based on $Ti_3C_2T_x$ MXene nanosheets. *Scientific Reports*. 7:1598. https://doi.org/10.1038/s41598-017-01714-3

21 Liu, L., Zschiesche, H., Antonietti, M., Daffos, B., Tarakina, N., Gibilaro, M., Chamelot, P., Massot, L., Duployer, B., Taberna, P.L., & Simon, P. (2023). Tuning the surface chemistry of MXene to improve energy storage: example of nitrification by salt melt. *Advanced Energy Materials*, 13, 2202709. https://doi.org/10.1002/aenm.202202709

22 Fagerli, F., Wang, Z., Grande, T., Kaland, H., Selbach, S.M., Wagner, N., & Wiik, K. (2022). Removing fluoride terminations from multilayered V_2CT_x MXene by gas hydrolyzation. *ACS Omega*, 7, 24656–24665. https://doi.org/10.1021/acsomega.2c02441

23 Lei, J., Yu, F., Xie, H., & Ma, J. (2023). $Ti_3C_2T_x$ MXene/carbon nanofiber multifunction electrode for electrodeionization with antifouling activity. *Chemical Science*, *14*(13), 3610–3621. https://doi.org/10.1039/d2sc06946f

24 Huang, L., Ding, L., & Wang, H. (2021). MXene-based membranes for separation applications. *Small Science*, 1, 2100013. https://doi.org/10.1002/smsc.202100013

25 Carey, M., & Barsoum, M.W. (2021). MXene polymer nanocomposites: a review. Materials Today Advances, 9, 100120. https://doi.org/10.1016/j.mtadv.2020.100120

26 Abbasi, F., Hajilary, N., & Rezakazemi, M. (2022). Antibacterial properties of MXene-based nanomaterials: a review. *Materials Express*, 12, 34–48. https://doi.org/10.1166/mex.2022.2138

27 Naguib, M., Unocic, R.R., Armstrong, B.L., & Nanda, J. (2015). Large-scale delamination of multilayer transition metal carbides and carbonitrides (MXenes). *Dalton Transactions*, 44, 9353–9358. https://doi.org/10.1039/C5DT01247C

28 Gentile, A., Marchionna, S., Balordi, M., Pagot, G., Ferrara, C., Noto, V., & Ruffo, R. (2022). Critical analysis of MXene production with in situ HF forming agents for sustainable manufacturing. *ChemElectroChem*, 9, e202200891. https://doi.org/10.1002/celc.202200891

29 Wang, Y., Xu, Y., Hu, M., Ling, H., & Zhu, X. (2020). MXenes: focus on optical and electronic properties and corresponding applications. *Nanophotonics*, 9, 1–24. https://doi.org/10.1515/nanoph-2019-0556

30 Ahmed, Z., Rehman, F.U., Ali, U., Ali, A., Iqbal, M., & Thebo, K.H. (2021). Recent advances in MXene-based separation membranes. *ChemBioEng Reviews*, 8, 1–12. https://doi.org/10.1002/cben.202000026

31 Thangavelu, H., Huang, C., Chabanais, F., Palisaitis, J., & Persson, P. (2025). A review on MXene terminations. *Advanced Functional Materials*, 36, 25015604. https://doi.org/10.1002/adfm.202515604

32 Kumar, S., Park, H., Kumar, M., & Seo, Y. (2023). Long-term stability studies and applications of $Ti_3C_2T_x$ MXene. *International Journal of Energy Research*, 2023, 5275439. https://doi.org/10.1155/2023/5275439

33 Lee, A., Shekhirev, M., Anayee, M., & Gogotsi, Y. (2024). Multi-year study of environmental stability of $Ti_3C_2T_x$ MXene films. *Graphene and 2D Materials*, 9, 1–9. https://doi.org/10.1007/s41127-024-00076-8

34 Jun, B.M., Kim, S., Heo, J., Park, C.M., Her, N.G., Jang, M., Huang, H., Han, J., & Yoon, Y. (2019). Review of MXenes as new nanomaterials for energy storage/delivery and selected environmental applications. *Nano Research*, 12, 471–487. https://doi.org/10.1007/s12274-018-2225-3

35 Kouao, D.S., & Siuzdak, K. (2025). Electrochemical synthesis of MXenes: a promising leap beyond hydrothermal MAX phase etching. *2D Materials*, 13, 012001. https://doi.org/10.1088/2053-1583/ae2a4d

36 Kruger, D., Garcia, H., & Primo, A. (2024). Molten salt derived MXenes: synthesis and applications. *Advanced Science*, 11, 2307106. https://doi.org/10.1002/advs.202307106

37 Berdiyorov, G., Madjet, M., & Mahmoud, K. (2021). First-principles density functional theory calculations of bilayer $Ti_3C_2T_x$ MXene/graphene and AgNP heterostructure membranes. *Membranes*, 11, 543. https://doi.org/10.3390/membranes11070543

38 Mahabari, K., Mohili, R.D., Patel, M., Jadhav, A.H., Lee, K., & Chaudhari, N.K. (2024). HF-free microwave-assisted synthesis of MXene as an electrocatalyst for hydrogen evolution in alkaline media. *Nanoscale Advances*, 6, 5388–5397. https://doi.org/10.1039/D4NA00250D

39 Feng, Y., Zhang, M., Yan, H., Zhang, Y., Guo, R., & Wang, H. (2022). Microwave-assisted efficient exfoliation of MXene and its composite for high-performance supercapacitors. *Ceramics International*, 48, 9518–9526. https://doi.org/10.1016/j.ceramint.2021.12.149

40 Mashangva, T.T., Vishwakarma, N., Singh, P.P., Prasher, S., Dhiman, R., Kumar, M., & Sharma, A. (2026). Synergistic enhancement of electrochemical properties in domestic microwave-assisted $Ti_3C_2T_x$ MXene composite with V_2O_5 nanoparticles for supercapacitor applications. *Journal of Energy Storage*, 150, 120387. https://doi.org/10.1016/j.est.2026.120387

41 Bagri, U., Jan, S., Sharma, A., & Singh, P.P. (2025). Enhanced photocatalytic degradation of ciprofloxacin from pharmaceutical wastewater using microwave-synthesized lanthanum/MXene nanocomposites. *Topics in Catalysis*. https://doi.org/10.1007/s11244-025-02214-9

42 Numan, A., Rafique, S., Khalid, M., Zaharin, H., Radwan, A., Mokri, N., Oh, P.C., & Rashmi, W. (2022). Microwave-assisted rapid MAX phase etching and delamination: A paradigm shift in MXene synthesis. *Materials Chemistry and Physics*, 288, 126429. https://doi.org/10.1016/j.matchemphys.2022.126429

43 Saha, A., Shpigel, N., Leifer, N., Taragin, S., Sharabani, T., Aviv, H., Perelshtein, I., Nessim, G., Noked, M., & Gogotsi, Y. (2021). Enhancing the energy storage capabilities of $Ti_3C_2T_x$ MXene electrodes by atomic surface reduction. *Advanced Functional Materials*, 31, 2106294. https://doi.org/10.1002/adfm.202106294

44 Liu, S., Zhou, Y., Zhou, J., Tang, H., Gao, F., Zhao, D., Ren, J., Wu, Y., Wang, Z., Luo, Y., Liu, X., & Zhang, Y. (2022). $Ti_3C_2T_x$ MXene-based flexible materials for electrochemical energy storage and solar energy conversion. *Nanophotonics*, 11, 3139–3164. https://doi.org/10.1515/nanoph-2022-0228

45 Liu, Y., Wang, Y., Wu, N., Han, M., Liu, W., Liu, J., & Zeng, Z. (2023). Diverse structural design strategies of MXene-based macrostructures for high-performance electromagnetic interference shielding. *Nano-Micro Letters*, 15, 203. https://doi.org/10.1007/s40820-023-01203-5

46 Hwang, H., Yang, S., Yuk, S., Lee, K.S., Byun, S., & Lee, D. (2023). $Ti_3C_2T_x$ MXene as a growth template for amorphous RuO_x in carbon nanofiber-based flexible electrodes for enhanced pseudocapacitive energy storage. *NPG Asia Materials*, 15, 76. https://doi.org/10.1038/s41427-023-00476-x

47 Jose, S., Price, J., Lopez, J., Perez-Perez, E., & Menezes, P. (2025). Advances in MXene materials: fabrication, properties, and applications. *Materials*, 18, 4894. https://doi.org/10.3390/ma18214894

48 Cai, Z., & Kim, H. (2025). Recent advances in MXene gas sensors: synthesis, composites, and mechanisms. *npj 2D Materials and Applications*, 9, 58. https://doi.org/10.1038/s41699-025-00586-w

49 Said, Z., Sohail, M., Tabassum, H., Sajid, I., Ali, H., Jamil, F., Mishra, Y.K., & Pandey, A. (2025). MXenes at the forefront: advances in energy storage and nanofluidic applications. *Advanced Composites and Hybrid Materials*, 8, 1404. https://doi.org/10.1007/s42114-025-01404-z

50 Silva, L., Fileti, E.E., & Colherinhas, G. (2025). Exploring MXene materials in energy storage devices: a review of supercapacitor applications. *ACS Materials Au*, 5, 1–18. https://doi.org/10.1021/acsmaterialsau.5c00102

51 Jawad, N., Darwesh, T., Abbas, A., Yahya, A.A., Hilal, A., Rashid, K., Abood, T., Al-Juboori, R., Meskher, H., & Al-Saadi, S. (2025). MXene synthesis, surface functionalization, and membrane integration for photocatalytic removal of heavy metals from wastewater. *Materials Today Sustainability*, 32, 101208. https://doi.org/10.1016/j.mtsust.2025.101208

52 Han, Y., Hu, J., Liu, X., & Liu, F. (2025). Progress in Surface and Interface Modification Strategies of MXene Materials for Energy Storage Applications. *Materials*, *18*(15), 3576. https://doi.org/10.3390/ma18153576

53 Li, H., Liu, L., Yuan, T., Zhang, J., Wang, T., Hou, J., & Chen, J. (2024). Advances in MXene surface functionalization strategies for CO_2 reduction. *Nanoscale*, *16*(24), 11480–11495. https://doi.org/10.1039/d4nr01517g

54 Koh, S.W., Rekhi, L., Arramel, A., Birowosuto, M.D., Trinh, T., Ge, J., Yu, W., Wee, A.T.S., & Li, C.H. (2024). Tuning the work function of MXene via surface functionalization. *ACS Applied Materials & Interfaces*, 16, 11234–11244. https://doi.org/10.1021/acsami.3c11857

55 Ganesan, S., Ethiraj, K., Kumar, K., & Palaniappan, A. (2022). Biomedical applications of MXenes. In: *MXene Materials*. Springer. https://doi.org/10.1007/978-3-031-05006-0_11

56 Bhattacharjee, Y., Mielke, L., Al-Hussein, M., Singh, S., Schaefer, K., Rodriguez-Barea, B., Li, Q., Ghosh, A.K., Erbe, A., Herrmann, C., Vaynzof, Y., Fery, A., & Schlicke, H. (2025). Molecular cross-linking of MXenes: tunable interfaces and chemiresistive sensing. *Advanced Functional Materials*, 35, 2501884. https://doi.org/10.1002/adfm.202518884

57 Shuck, C.E., Sarycheva, A., Anayee, M., Levitt, A., Zhu, Y., Uzun, S., Balitskiy, V., Zahorodna, V., & Gogotsi, Y. (2020). Scalable synthesis of $Ti_3C_2T_x$ MXene. *Advanced Engineering Materials*, 22, 1901241. https://doi.org/10.1002/adem.201901241

58 Gentile, A., Marchionna, S., Balordi, M., Pagot, G., Ferrara, Ch., Di Noto, V., & Ruffo, R. (2022). Critical Analysis of MXene Production with In-Situ HF Forming Agents for Sustainable Manufacturing. *ChemElectroChem*, *9*(23). https://doi.org/10.1002/celc.202200891

59 Lee, A., Shekhirev, M., Anayee, M. & Gogotsi, Y. (2024). Multi-year study of environmental stability of $Ti_3C_2T_x$ MXene films. *Graphene and 2D Materials*, 9, 77–85. https://doi.org/10.1007/s41127-024-00076-8

60 Kiran, N.U., Deore, A., More, M., Raye, D., Rout, C.S., Mane, P., Chakraborty, B., Besra, L., & Chatterjee, S. (2022). Comparative study of cold electron emission from 2D $Ti_3C_2T_x$ MXene nanosheets with respect to its precursor Ti_3SiC_2 MAX phase. *ACS Applied Electronic Materials*, *4*(6), 2656–2666. https://doi.org/10.1021/acsaelm.2c00128

61 Solangi, M.Y., Hanan, A., Aftab, U., Soomro, I.A., & Ibupoto, Z.H. (2025). Novel titanium carbide ($Ti_3C_2T_x$) MXene electrocatalyst for HER application. *NUST Journal of Engineering Sciences*, *18*(1). https://journals.nust.edu.pk/index.php/njes/issue/view/35

62 Fu, S., Zhou, Q., Jin, C., Gao, Z., Niu, M., Wan, D., & Bao, Y. (2025). Interface protection mechanism of Ti_3AlC_2 ceramics under CMAS corrosion condition. *International Journal of Applied Ceramic Technology*, 22, e15134. https://doi.org/10.1111/ijac.15134

63 Bagheri, S., Lipatov, A., Vorobeva, N.S., & Sinitskii, A. (2023). Interlayer Incorporation of A-Elements into MXenes Via Selective Etching of A′ from $M_{n+1}A'_{1-x}A''_xC_n$ MAX Phases. *ACS Nano*, 17, 18747–18757. https://doi.org/10.1021/acsnano.3c02198

64 Ahmed, E.M., Ali, A.S., Hieba, E.M., Shaban, Z.S., Fathy, M.S., Amer, A.M., Ishmael, A.M., Bakr, A., Rashdan, H.R.M., & Elzwawy, A. (2025). Exploring the potential of MXenes in advanced energy, environmental, and biomedical applications. *RSC Advances*, 15, 44812–44863. https://doi.org/10.1039/D5RA04498G

65 Mashtalir, O., Naguib, M., Mochalin, V.N., Dall'Agnese, Y., Heon, M., Barsoum, M.W., & Gogotsi, Y. (2013). Intercalation and Delamination of Layered Carbides (MXenes). *Nature Communication*, 4, 1716. https://doi.org/10.1038/ncomms2715

66 Lipatov, A., Goad, A., Loes, M.J., Vorobeva, N.S., Abourahma, J., Gogotsi, Y., & Sinitski, A. (2021). High electrical conductivity and breakdown current density of individual monolayer $Ti_3C_2T_x$·MXene flakes. *Matter*, *4*(4), 1413–1427. https://doi.org/10.1016/j.matt.2021.01.021

67 Magnuson, M. & Mattesini, M. (2017). Chemical bonding and electronic-structure in MAX phases as viewed by X-ray spectroscopy and density functional theory. *Thin Solid Films*, 621, 108–130. https://doi.org/10.1016/j.tsf.2016.11.005

68 Long, Y., Tao, Y., Shang, T., Yang, H., Sun, Z., Chen, W. & Yang, Q. (2022). Roles of Metal Ions in MXene Synthesis, Processing and Applications: A Perspective. *Advanced Science*, 9, 2200296. https://doi.org/10.1002/advs.202200296

69 Alhabeb, M., Maleski, K., Anasori, B., Lelyukh, P., Clark, L., Sin, S., & and Gogotsi, Y. (2017). Guidelines for Synthesis and Processing of Two-Dimensional Titanium Carbide ($Ti_3C_2T_x$·MXene). *Chemistry of Materials*, 29, 7633−7644. https://doi.org/10.1021/acs.chemmater.7b02847